Current Biology 23, 2146–2150, November 4, 2013 ©2013 Elsevier Ltd All rights reserved http://dx.doi.org/10.1016/j.cub.2013.08.057

Report

Temporal Jitter of the BOLD Signal Reveals a Reliable Initial Dip and Improved Spatial Resolution

Masataka Watanabe,[1,2,3,*] Andreas Bartels,[2,4,*] Jakob H. Macke,[5] Yusuke Murayama,[2] and Nikos K. Logothetis[2,6]

[1]School of Engineering, University of Tokyo, 113-0033 Tokyo, Japan

[2]Max Planck Institute for Biological Cybernetics, 72076 Tübingen, Germany

[3]RIKEN Brain Science Institute, Wako, 351-0198 Saitama, Japan

[4]Vision and Cognition Lab, Centre for Integrative Neuroscience, University of Tübingen, 72076 Tübingen, Germany

[5]Neural Computation and Behaviour Group, Max Planck Institute for Biological Cybernetics and Bernstein Center for Computational Neuroscience, 72076 Tübingen, Germany

[6]Imaging Science and Biomedical Engineering, University of Manchester, Manchester M13 9PL, UK

Summary

fMRI, one of the most important noninvasive brain imaging methods, relies on the blood oxygen level-dependent (BOLD) signal, whose precise underpinnings are still not fully understood [1]. It is a widespread assumption that the components of the hemodynamic response function (HRF) are fixed relative to each other in time, leading most studies as well as analysis tools to focus on trial-averaged responses, thus using or estimating a condition- or location-specific "canonical HRF" [2–4]. In the current study, we examined the nature of the variability of the BOLD response and asked in particular whether the positive BOLD peak is subject to trial-to-trial temporal jitter. Our results show that the positive peak of the stimulus-evoked BOLD signal exhibits a trial-to-trial temporal jitter on the order of seconds. Moreover, the trial-to-trial variability can be exploited to uncover the initial dip in the majority of voxels by pooling trial responses with large peak latencies. Initial dips exposed by this procedure possess higher spatial resolution compared to the positive BOLD signal in the human visual cortex. These findings allow for the reliable observation of fMRI signals that are physiologically closer to neural activity, leading to improvements in both temporal and spatial resolution.

Results

Trial-to-Trial Temporal Jitter of the BOLD Positive Peak

In the first experiment, we investigated the trial-to-trial temporal variability of the positive blood oxygen level-dependent (BOLD) peak in the human visual cortex using an event-related visual stimulation paradigm with long poststimulus periods. A polar-transformed checkerboard (width: 18 degrees visual angle, duration: 4 s; Figure 1A) was presented centrally with randomized interstimulus intervals of 40–46 s to obtain visually evoked fMRI BOLD responses compared to baseline (see Experimental Procedures). In order to quantify the latency of the peak of the positive BOLD response for a given trial, we defined it as the time of the highest BOLD signal of the temporally smoothed and detrended BOLD time course relative to stimulus onset. Figure 1B plots the standard deviation of the detected peak latencies in relation to the width of the Gaussian kernel used for temporal smoothing. Hereafter, we use the Gaussian kernel width value of 3.8 s that resulted in the smallest trial-to-trial variability of positive peak latencies, which nevertheless amounted to a considerable 4.1 s SD. Figure 1C shows trial-by-trial response time courses of a single voxel, sorted by positive BOLD signal peak latencies. Also, here the peak latency of the BOLD response varied in the range of several seconds. This was typical for most visually responsive voxels and can be quantified by the SD of the peak times that ranged between 2 and 5 s. (For further analysis showing evidence that the BOLD temporal jitter has a biological origin, see Figure S1 available online.)

The Jitter-Uncovered Initial Dip

When single-trial responses of BOLD signal were sorted according to their positive peak latency, we saw two negative response components that are independent of the temporal shift of the positive BOLD signal. Figure 2A shows averaged responses, pooled from trials with different peak latency ranges. Each curve contains data from the same set of voxels, but from different trials, revealing two response properties. First the so-called initial dip, i.e., the early negative component of the BOLD response, is clearly visible in trials with long peak latencies (hereafter termed the "jitter-uncovered initial dip"). Second, a sharp postresponse undershoot becomes apparent in trials with short peak latencies. Interestingly, both properties are cancelled out in the average response across all trials (black line in Figure 2A). The same procedure, applied to data of a single voxel, is illustrated in Figure 2B. Although this voxel does not show the initial dip when all trials are averaged, it can be detected when only the 50% of trials with late BOLD peak are considered.

In the following, we examine the fundamental properties of the jitter-uncovered initial dip in voxelwise analyses in which we relate its magnitude to that of the conventional initial dip, to the positive peak amplitude, and to the positive peak latency, using data obtained from the first human experiment. Scatterplots of the magnitudes of dips detected conventionally (all-trial average) or using jitter analysis are shown for a representative subject in Figure 2C. Results show that the magnitude of the jitter-uncovered initial dip was on average larger than that of the conventional initial dip, which was significant for every subject (pairwise t test; $p < 1.0 \times 10^{-8}$). The widths of the temporal window were optimized to maximize the number of voxels classified as having the particular type of initial dip. The magnitude of the jitter-uncovered initial dip was defined as the percent signal change between 3 s prior and 3 s after stimulus onset using only the 50% of trials with late BOLD peak responses, i.e., late-peaking trials (Figure 2B). In contrast, the conventional initial dip was defined as the

*Correspondence: watanabe@tuebingen.mpg.de (M.W.), andreas.bartels@tuebingen.mpg.de (A.B.)

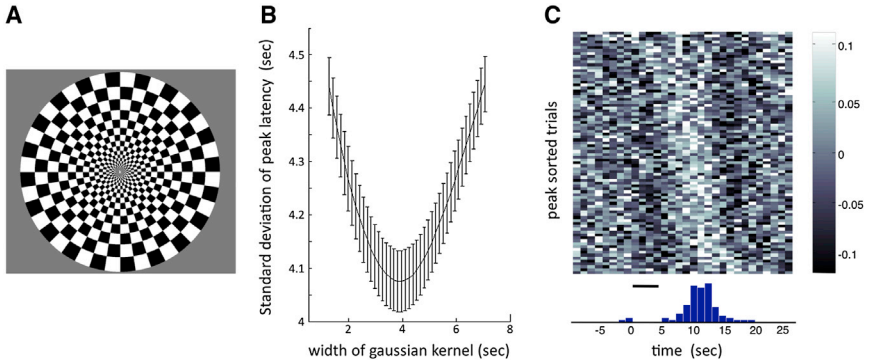

Figure 1. Temporal Fluctuation of BOLD Positive Peak Signal Latency

(A) Full-field checker stimulus used for experiment 1, which flickered at 4 Hz during 4 s, followed by 40–46 s blank.

(B) Dependency of the standard deviation of BOLD peak latencies on the width of the temporal smoothing Gaussian kernel used for peak detection. Error bars denote 95% confidence interval.

(C) BOLD time courses (aligned to the stimulus onset) of a representative voxel, trial sorted by the latency of the positive peak. Time histogram of peak latencies is shown in the lower panel.

See also Figure S1.

percent signal change between 3 s prior and 1.5 s after stimulus onset using all trial responses.

Figures 2D and 2E show scatterplots of jitter-uncovered dip magnitude versus positive peak amplitude and peak latency, respectively. Peak amplitude (Figure 2D) and peak latency (Figure 2E) were both negatively correlated with the jitter-uncovered initial dip magnitude ($p < 1.0 \times 10^{-8}$) for all six subjects and each type of correlation. These negative correlations are likely due to the voxel-by-voxel variability in terms of overlap with drainage vessels; voxels with large BOLD amplitudes and large peak latencies tend to have a large signal contribution from large drainage vessels, and therefore the initial dip that originates from tissue deoxygenation and/or dilation of arterioles [5, 6] becomes relatively smaller. Note here that the vascular composition within a voxel is a fixed anatomical property, whereas the trial-to-trial temporal jitter reflects fluctuations in neural states, neurovascular coupling, and variable vascular responses across trials. (For experimental evidence showing that the jitter-uncovered initial dip is robust compared to the conventional initial dip also in the motor cortex, see Figure S2.)

The Jitter-Uncovered Initial Dip Leads to Higher Spatial Resolution in the Human Visual Cortex

Previous studies have shown that the positive component of the BOLD response has a substantial point spread, i.e., a spatial spill-out of the response beyond the site of neural activation [7]. In contrast, the initial dip of the BOLD signal is considered to be more confined in space [8–11]. The primary reason for the high interest of neuroscientists in the initial dip has been that in theory, it may be more closely related to the site of neural metabolism and thus allow for more precise spatial localization compared to the positive BOLD peak. The aim of the second experiment was to validate the identification of the initial dip that was revealed by the jitter analysis and to determine whether it indeed has a better spatial confinement to the locus of neural activation compared to the positive component of the BOLD response.

In order to obtain a reliable estimate, we placed fMRI slices tangential to the calcarine sulcus of V1, which would allow two-dimensional sampling of BOLD activity from a flat gray-matter region (Figure 3B). Two eccentric rings were used as visual stimuli, with shared stimulus borders (Figure 3A). The eccentricity of the shared stimulus border was adjusted between 3 and 6 degrees so that the activity border centered on the flat gray-matter region.

Figures 3C and 3D present activity maps of a representative subject obtained by analysis based on the positive BOLD peak and the jitter-uncovered initial dip, respectively. The two values were calculated according to the methods provided in the previous experiment. Red and green color scales correspond to activities evoked by the two eccentric rings, and additive use of color scales leads to yellow representing overlap. The positive BOLD analysis resulted in an overlap of activity with a width of several voxels (note that we used 1.5 mm in-plane resolution), whereas the jitter-uncovered initial dip analysis yielded minimal overlap.

To quantify the above observation, we calculated the point spread function (see Experimental Procedures). Signal fall-off as a function of the distance from the activation border is shown in Figure 3F, where red and blue lines denote point spread functions of the positive BOLD peak and the jitter-uncovered initial dip, respectively. Hatched regions indicate 95% confidence intervals. The two types of activity differed for all distances larger than 1 mm from the activity border ($p < 0.05$, t test). The estimated point spread functions provide clear evidence that the jitter-uncovered initial dip results in enhanced spatial resolution compared to the positive BOLD peak, with about 2 mm point spread function compared to about double of that in the positive BOLD peak. Furthermore, the sharp monotonic decrease of point spread right from the border of the stimulus, compared to the blunt point spread of the positive BOLD, has the potential to drastically decrease the size of the minimal resolvable functional structure in combination with differential mapping and smaller voxel sizes at higher field strengths, which will be an exciting future application of this method. However, note that the increase in spatial resolution comes at the cost of poorer signal-to-noise ratio. (For further experimental evidence on the spatial confinement of the jitter-uncovered initial dip, including voxel population analysis, see Figure S3.)

Discussion

We examined trial-by-trial temporal fluctuations of BOLD responses in the human visual and motor cortices. Results show that the delay of the positive peak BOLD response fluctuated on the order of seconds. Furthermore, we found two negative components of the BOLD response that were not affected by the temporal jitter of the positive component: a robust initial dip and a sharp poststimulus undershoot. The initial dip was reliably brought to light in most single voxels by pooling those trial responses that had long positive peak latencies. In contrast, when all trials were pooled regardless of the peak latency, the initial dip was seen only in a minority of voxels. The latter result is in line with previous studies reporting the elusive nature of the conventional BOLD initial dip [12–14]. By employing two spatially complementary visual stimuli designed to activate retinotopically segregated regions

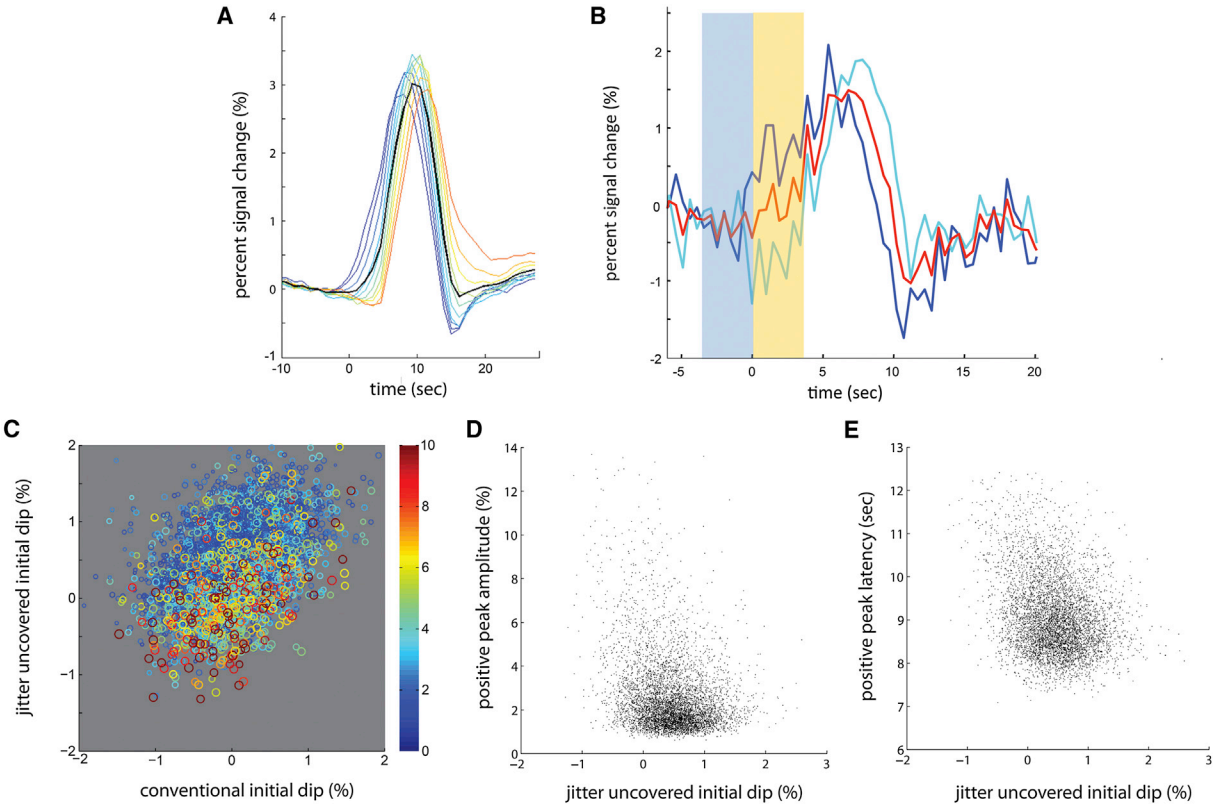

Figure 2. Properties of the Jitter-Uncovered Initial Dip

(A) Average BOLD time courses from the same pool of voxels. Each curve contains data from the same set of voxels, but from trials with different latencies of the positive peak. Black line indicates average response across all trials. Colored lines indicate average responses of subsets of trials with increasing latencies of their response peak.

(B) Average time courses obtained from a single representative voxel. Red line indicates average across all trials. Light blue and dark blue lines indicate 50% of trials with late and early positive peak latencies, respectively. Shaded regions in blue and yellow denote the time windows of averaging for prestimulus BOLD level and the jitter-uncovered initial dip, respectively.

(C) Voxelwise scatterplots of the magnitudes of the conventional initial dip and the jitter-uncovered initial dip of a representative subject. Positive values indicate a decrease in BOLD signal. Each marker represents a single voxel. Marker color indicates the percent signal change of the positive BOLD peak (averaged across all trials), whereas marker size indicates the positive peak latency (averaged across all trials). The magnitude of the jitter-uncovered initial dip was on average larger than that of the conventional initial dip, which was significant for every subject (pairwise t test; $p < 1.0 \times 10^{-8}$).

(D) Voxelwise scatterplots of jitter-uncovered initial dip magnitude and percent signal change of the positive BOLD peak of a representative subject.

(E) Voxelwise scatterplots of jitter-uncovered initial dip magnitude and positive peak latency of a representative subject. (D) and (E) show negative correlations ($p < 1.0 \times 10^{-8}$) for all six subjects likely due to the voxel-by-voxel variability in terms of overlap with drainage vessels (see main text).

See also Figure S2.

of the visual cortex, our novel analysis showed that the early negative response was better colocalized to neuronal activity compared to traditional analysis based on the positive BOLD response.

First, we discuss neurovascular mechanisms underlying the initial dip with regard to the proposed method of the jitter-uncovered initial dip. One congruent observation from intrinsic optical imaging (IOI) studies is that there is a point in time after stimulus presentation where the tissue remains dark (due to raised deoxyhemoglobin [HbR] concentration, but see [5]) while portions of visible vasculature are brightening (higher HbO_2 concentration) (Figure 1D in [15]; Figure 1B in [5]; Figure 2A in [16]). The darkening reveals a columnar structure, and hence it is colocalized to neural activity, whereas the subsequent tissue brightening has a much larger spatial scale and does not follow the functional structure. Furthermore, if we assume that the onset of vasculature brightening has a trial-by-trial variability, and taking into account the opposite effects in tissue and vasculature observed in IOI, as well as the fact that both are spatially pooled in single fMRI voxels, it becomes apparent why the fMRI initial dip was only robustly revealed when pooling responses with large positive peak latencies (Figure 4). Inclusion of short-latency positive peak trials would have allowed the signal related to early vascular oxygenation to cancel that of the local deoxygenation of tissue within single voxels. In relation, it will be an important question for future studies to examine to which extent the variability in trialwise fluctuations of BOLD peak latencies is related either to preceding neural activity (with potential correlates in cognition and perception) [17–19] or to physiological mechanisms of neurovascular coupling.

The point spread of neural activity itself has been estimated to be 2–3 mm using optical imaging with voltage-sensitive dyes [20, 21]. This is in good agreement with our estimation of the point spread function of the jitter-uncovered initial dip. The important point, in terms of future applications of the fMRI BOLD jitter-uncovered initial dip, is that compared to the positive component, the amplitude of the initial dip drops

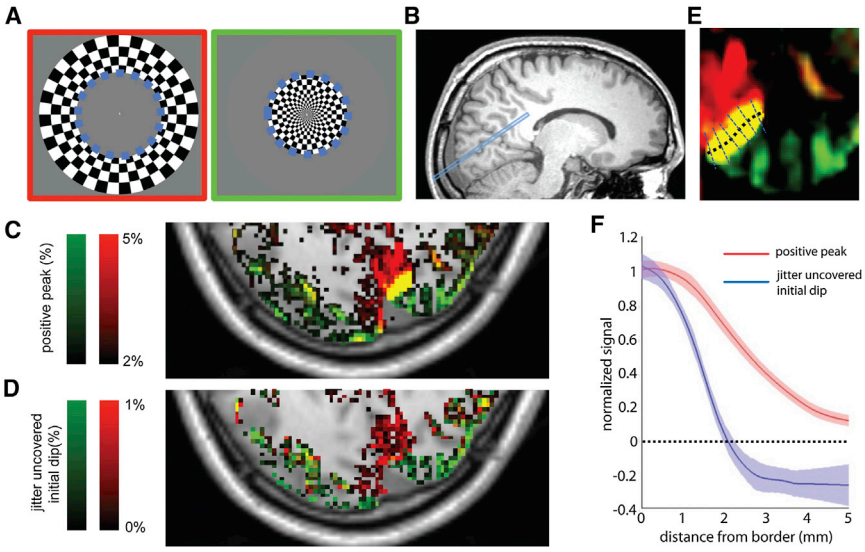

Figure 3. Comparison of the Point Spread Function between the Jitter-Uncovered Initial Dip and the BOLD Positive Peak

(A) Complementary visual stimuli (flickering at 4 Hz) used for experiment 2. Surrounding colored squares (red: larger eccentric ring, green: small eccentric ring) and dashed blue circles (shared border) are shown only for illustrative purposes.

(B) Scan slice aligned to the calcarine sulcus.

(C and D) Activation map obtained using the positive BOLD peak (C) and the jitter-uncovered initial dip (D). Green and red color scales correspond to activity evoked by the two visual stimuli shown in (A).

(E) Oversampled (linear interpolation) activation map (positive BOLD peak) used to calculate the point spread function. The thick dashed line denotes the estimated activation border, and the thin dashed lines denote the lines orthogonal to the activation border where activation was sampled for calculating the point spread function.

(F) Point spread functions of the positive BOLD peak and the jitter-uncovered initial dip. Shaded regions indicate 95% confidence interval.

See also Figure S3.

sharply and monotonically with cortical distance as in the results of voltage-sensitive dye imaging [21]. This would allow resolving functional structures much smaller than 2–3 mm, as seen in intrinsic optical imaging studies that reveal functional structures at the spatial scale of 100–200 μm [22]. Hence, although the current results are limited by voxel size and signal-to-noise ratio achievable by a standard 3 T MRI scanner, jitter-uncovered initial dip imaging will allow taking full advantage of future developments in MRI hardware and lead to noninvasive observation of functional structures with unprecedented spatial resolution.

Experimental Procedures

Experiment 1: Human fMRI BOLD Experiment with Full-Field Visual Stimulus

Subjects

Six healthy right-handed volunteers (three males and three females), age 27 ± 3 years, participated in the experiment. All subjects had

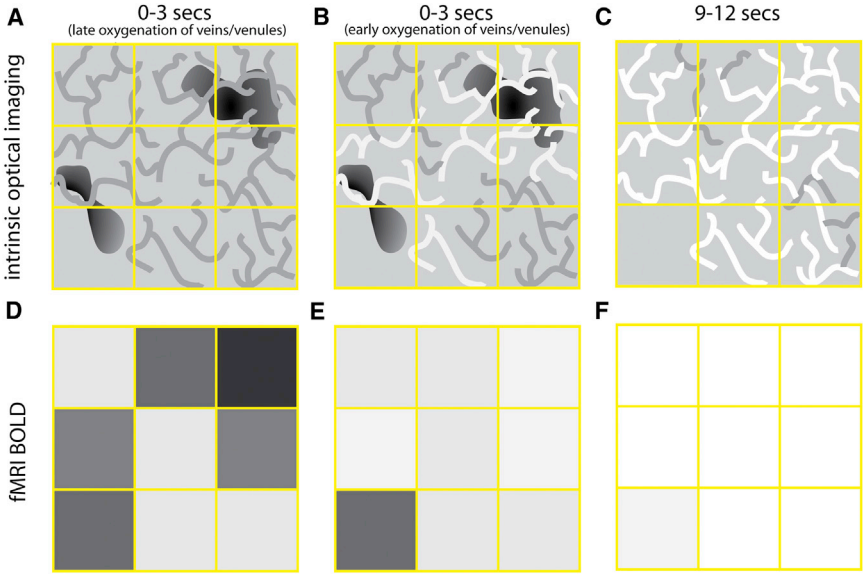

Figure 4. Schematic Illustration Relating the Jitter-Uncovered Initial Dip to Vascular Responses Accounting for Its Higher Spatial Resolution

(A–C) Illustration of intrinsic optical imaging data in two possible states of early phases (A and B; 0–3 s after stimulus onset) and in a late phase (C; 9–12 s after stimulus onset). Dark patches on the upper right and the lower left corners in (A) and (B) correspond to regions with increased absorbed light due to increase in local neural activity and correspondingly increased deoxyhemoglobin (HbR). Curved lines denote visible veins and venules. (A) illustrates an example trial case with late oxygenation (increase in HbO_2), depicted prior to oxygenation in veins and venules, whereas (B) illustrates an example trial case with early oxygenation. An illustration of a late phase is shown in (C), where both local and remote veins and venules are oxygenated regardless of the onset of oxygenation. Yellow squares denote virtual borders corresponding to hypothetical fMRI voxels.

(D–F) Corresponding fMRI voxel activation pattern during the early phase (D, late oxygenation trial case; E, early oxygenation trial case) and during the late phase (F). When there is no early oxygenation of veins and venules, voxel signal values reflect the local darkening patch (D), whereas in the case of early oxygenation, voxel signal values are mostly affected by the oxygenation in the veins and venules (i.e., reduction of HbR) that have larger signal contribution to the gradient echo BOLD signal (E). If all trials were to be averaged together, as in the method of calculating the conventional initial dip, the local decrease of BOLD seen in late oxygenation trials (e.g., D) would be cancelled out by the increase of BOLD in trials with early oxygenation (e.g., E). Here, only the voxels with small contribution of veins and venules (lower left voxel) would not suffer from the cancellation effect and show a conventional initial dip. In contrast, the proposed method of the jitter-uncovered initial dip would take only averages of late oxygenation trials (e.g., D), and hence the voxel pattern would reflect the darkened patches in intrinsic optical imaging that correspond to local increase in neural activity. (C) and (F) explain why positive BOLD signal has a comparably larger point spread function. That is, drainage veins and vessels are connected horizontally along the cortical surface and oxygenation propagates to remote regions.

normal or corrected-to-normal visual acuity and normal stereo-depth perception. All subjects gave prior written informed consent before each experiment, and the study was approved by the local joint ethics committee of the Max Planck Institute and the University Clinic Tübingen.

MRI Acquisition and Stimulus Presentation

Functional images were acquired on a 3 T Siemens TIM scanner located in the Max Planck Institute Tübingen with a gradient echo planar imaging pulse sequence and a 12-channel phased-array head coil. We collected 14 slices (slice thickness 2 mm) oriented perpendicular to the individual subject's calcarine sulcus with the first slice prescribed at the occipital pole, using an interleaved sequence and the following parameters: volume repetition time (TR) 1.16 s, echo time (TE) 35 ms, 88 × 128 matrix, voxel size 1.5 × 1.5 × 2.0 mm. A set of high-resolution (1 mm isotropic) T1-weighted 3D modified driven equilibrium Fourier transform (MDEFT) images was acquired from each subject as an anatomical reference. All stimuli were programmed in MATLAB in the PsychToolbox environment [23, 24]. See Supplemental Experimental Procedures for further description of stimulus presentation.

Data Analysis

fMRI data were preprocessed using SPM5 (Wellcome Department of Cognitive Neurology, London; http://www.fil.ion.ucl.ac.uk/spm). Preprocessing included image realignment and coregistration of functional and anatomical images. A general linear model (GLM) analysis with a boxcar regressor was applied to calculate the statistical values used to determine visually activated voxels in the occipital cortex ($p < 0.05$, family-wise error corrected). No spatial smoothing was applied on the functional images.

Experiment 2: Human fMRI BOLD Experiment with Complementary Ring Stimuli and Cortical Tangential Scan

This experiment was identical to experiment 1, with the following differences. Subjects were five healthy right-handed volunteers (two males and three females), age 23 ± 3 years. Stimuli consisted of two sets of polar-transformed checkerboard rings with shared borders as shown in Figure 3A (100% contrast, shared border eccentricity adjusted between 3 and 6 degrees visual angle), flickering (contrast inversing) at 4 Hz. See Supplemental Experimental Procedures for further description of the stimulus presentation.

Data Analysis

We used the following procedure to estimate the point spread functions of the positive BOLD peak and the jitter-uncovered initial dip, respectively. First, the activation maps were oversampled by a factor of ten using linear interpolation to determine the border of the two activation patches evoked by two ring stimuli. The border was defined as a set of points in oversampled space along where the difference between the two activation patches became minimal (Figure 3E, thick dashed line). Next, for each of the border points, an activity profile was sampled along a straight line orthogonal to the border curve. For each subject, two point spread functions (inner to outer ring and outer to inner ring) were calculated by averaging the normalized activity profiles (normalized by the activation value at the border point). These were pooled across subjects and then averaged to obtain the subject averaged point spread function ($n = 5 \times 2$).

Supplemental Information

Supplemental Information includes three figures and Supplemental Experimental Procedures and can be found with this article online at http://dx.doi.org/10.1016/j.cub.2013.08.057.

Acknowledgments

This work was supported by the Max Planck Society and by the Centre for Integrative Neuroscience (EXC307), Tübingen. J.H.M. was funded by the research program of the Bernstein Center for Computational Neuroscience, Tübingen, of the German Federal Ministry of Education and Research (BMBF; FKZ: 01GQ1002). We thank D. Voinescu for assistance with data collection and D. Omer for discussions.

Received: August 12, 2013
Revised: August 26, 2013
Accepted: August 27, 2013
Published: October 17, 2013

References

1. Logothetis, N.K. (2008). What we can do and what we cannot do with fMRI. Nature *453*, 869–878.
2. Friston, K.J., Ashburner, J.T., Kiebel, S.J., Nichols, T.E., and Penny, W.D., eds. (2007). Statistical Parametric Mapping: The Analysis of Functional Brain Images (New York: Academic Press).
3. Boynton, G.M., Engel, S.A., Glover, G.H., and Heeger, D.J. (1996). Linear systems analysis of functional magnetic resonance imaging in human V1. J. Neurosci. *16*, 4207–4221.
4. Buxton, R.B., Wong, E.C., and Frank, L.R. (1998). Dynamics of blood flow and oxygenation changes during brain activation: the balloon model. Magn. Reson. Med. *39*, 855–864.
5. Sirotin, Y.B., Hillman, E.M., Bordier, C., and Das, A. (2009). Spatiotemporal precision and hemodynamic mechanism of optical point spreads in alert primates. Proc. Natl. Acad. Sci. USA *106*, 18390–18395.
6. Uludag, K. (2010). To dip or not to dip: reconciling optical imaging and fMRI data. Proc. Natl. Acad. Sci. USA *107*, E23–E23, author reply E24.
7. Shmuel, A., Yacoub, E., Chaimow, D., Logothetis, N.K., and Ugurbil, K. (2007). Spatio-temporal point-spread function of fMRI signal in human gray matter at 7 Tesla. Neuroimage *35*, 539–552.
8. Ernst, T., and Hennig, J. (1994). Observation of a fast response in functional MR. Magn. Reson. Med. *32*, 146–149.
9. Hu, X., Le, T.H., and Uğurbil, K. (1997). Evaluation of the early response in fMRI in individual subjects using short stimulus duration. Magn. Reson. Med. *37*, 877–884.
10. Kim, D.S., Duong, T.Q., and Kim, S.G. (2000). High-resolution mapping of iso-orientation columns by fMRI. Nat. Neurosci. *3*, 164–169.
11. Menon, R.S., Ogawa, S., Hu, X., Strupp, J.P., Anderson, P., and Uğurbil, K. (1995). BOLD based functional MRI at 4 Tesla includes a capillary bed contribution: echo-planar imaging correlates with previous optical imaging using intrinsic signals. Magn. Reson. Med. *33*, 453–459.
12. Moon, C.H., Fukuda, M., Park, S.H., and Kim, S.G. (2007). Neural interpretation of blood oxygenation level-dependent fMRI maps at submillimeter columnar resolution. J. Neurosci. *27*, 6892–6902.
13. Silva, A.C., Lee, S.P., Iadecola, C., and Kim, S.G. (2000). Early temporal characteristics of cerebral blood flow and deoxyhemoglobin changes during somatosensory stimulation. J. Cereb. Blood Flow Metab. *20*, 201–206.
14. Logothetis, N. (2000). Can current fMRI techniques reveal the microarchitecture of cortex? Nat. Neurosci. *3*, 413–414.
15. Grinvald, A., Slovin, H., and Vanzetta, I. (2000). Non-invasive visualization of cortical columns by fMRI. Nat. Neurosci. *3*, 105–107.
16. Chen, L.M., Friedman, R.M., Ramsden, B.M., LaMotte, R.H., and Roe, A.W. (2001). Fine-scale organization of SI (area 3b) in the squirrel monkey revealed with intrinsic optical imaging. J. Neurophysiol. *86*, 3011–3029.
17. Sadaghiani, S., Hesselmann, G., Friston, K.J., and Kleinschmidt, A. (2010). The relation of ongoing brain activity, evoked neural responses, and cognition. Front Syst Neurosci *4*, 20.
18. Britz, J., and Michel, C.M. (2011). State-dependent visual processing. Front. Psychol. *2*, 370.
19. Harvey, B.M., Vansteensel, M.J., Ferrier, C.H., Petridou, N., Zuiderbaan, W., Aarnoutse, E.J., Bleichner, M.G., Dijkerman, H.C., van Zandvoort, M.J., Leijten, F.S., et al. (2013). Frequency specific spatial interactions in human electrocorticography: V1 alpha oscillations reflect surround suppression. Neuroimage *65*, 424–432.
20. Grinvald, A., Lieke, E.E., Frostig, R.D., and Hildesheim, R. (1994). Cortical point-spread function and long-range lateral interactions revealed by real-time optical imaging of macaque monkey primary visual cortex. J. Neurosci. *14*, 2545–2568.
21. Chen, Y., Geisler, W.S., and Seidemann, E. (2006). Optimal decoding of correlated neural population responses in the primate visual cortex. Nat. Neurosci. *9*, 1412–1420.
22. Bonhoeffer, T., and Grinvald, A. (1993). The layout of iso-orientation domains in area 18 of cat visual cortex: optical imaging reveals a pinwheel-like organization. J. Neurosci. *13*, 4157–4180.
23. Pelli, D.G. (1997). The VideoToolbox software for visual psychophysics: transforming numbers into movies. Spat. Vis. *10*, 437–442.
24. Brainard, D.H. (1997). The Psychophysics Toolbox. Spat. Vis. *10*, 433–436.